Indian Journal of Chemistry
Vol. 61, March 2022, pp. 263-277

Heterocyclic ligated Co(II), Ni(II), Cu(II) and Zn(II) complexes for efficient photocatalytic and biological applications

R Selwin Joseyphus[a,*], Reshma R[a,b] & D Arish[c]

[a]Department of Chemistry, Mar Ivanios College (Autonomous), Nalanchira, Thiruvananthapuram 695 015, Kerala, India

[b]Department of Chemistry, SreeNarayana College, Varkala 695 145, Kerala, India

[c]Department of Glass Processing, FunGlass, Alexander Dubček University of Trenčín, Trenčín 91150, Slovakia

*E-mail: selwin.joseyphus@mic.ac.in

Received 02 October 2021; revised and accepted 18 February 2022

We report the synthesis and characterization techniques of mononuclear, heterocyclic ligated Co(II), Ni(II), Cu(II) and Zn(II) complexes. These heterocyclic derivatives, Schiff base (indal-2-abu), are obtained from the reaction between indole-3-carboxaldehyde (indal) and 2-aminobutyric acid (2-abu). From the fundamental analysis, it has been found that the Schiff base with the aforementioned metal ions forms four coordinated mononuclear complexes on 1:2 (metal:ligand) stoichiometry. The structural changes of the complexes are analyzed by FT-IR, electronic and magnetic analysis. The photocatalytic dye degradation activity study of the compounds is performed under UV-light using methylene blue (MB) dye. All the complexes are found to be excellent catalysts for the degradation of MB. Molecular docking is used to recognize the energetic site of the receptor, and attain the finest geometry of the ligand-receptor complex. Furthermore, antimicrobial investigations of Schiff base and its complexes are tested and the results are discussed in detail.

Keywords: Indal, Photocatalytic, Schiff base, Antimicrobial

The incredible growth in the area of bioinorganic chemistry has increased the importance of Schiff base (SB) complexes since it has been familiar that many of these complexes may serve as models for biologically significant species[1]. The SB complexes are primarily tested for their pharmaceutical uses and some of them are found to be effective and exist as drugs[2]. Currently, pharmaceutical compounds bearing metal ions in their structural backbone have received considerable attention in medicine[3]. Due to their excellent photocatalytic nature, recently, metal complexes could also be a potential candidate for the degradation of organic pollutants/persistent organic dyes[11-13]. Metal complexes of amino acids play a key role in the biological systems, for their physiological and catalytic reactions. α-amino acid residues exhibit various functions in biological systems[6-8]. The side-chain groups are very important for the creation of the metal centre and its catalytic action in proteins[9]. They are involved in metal binding, molecular recognition by weak interactions, enzyme catalysis, and formation of the molecular environment[10]. Apart from the biological systems, notably, it has been reported that SB can be used as a ligand (alternatives to phosphines) in Suzuki–Miyaura reactions[11,12].

Considering various ligand systems, the main drawback is toxicity, sensitivity to air, handling problems, and of course high costs. As mentioned earlier, since amino acid SB systems can be act as catalyst in the biological systems and beyond, some interesting amino-acid SB metal complexes may be prepared and their catalytic properties can be tested. Moreover, amino acid based systems can form stable chelate complexes with various metal ions through the amine and carboxylate moieties (NO-chelation). The properties of the amino acid can often be modified by using simple condensation reaction with aldehydes. Although many aldehydes have focused, the heterocyclic group containing aldehydes are very scarcely studied, but, interested in the perspective of tuning and improving their catalytic properties[13-15].

Indole plays an important role in the synthesis of new pharmaceutical products. Indole derivatives remain too remarkable in a great pact of interest in coordination and organometallic chemistry because the presence of hetero atoms may introduce major variations on the chemical, physical, photo-optical properties and catalytic or biological activities of this type of compounds[16]. In the present work, heterocyclic SB (indal-2-abu) ligand was synthesized

from indal with 2-abu and its Co/Ni/Cu/Zn(II) complexes were synthesized and structurally characterized. The photocatalytic efficiency, Molecular docking (MD) and biological studies were also studied in detail.

Experimental Details

Chemicals

Indole-3-carboxaldehyde and 2-aminobutyric acid were obtained from Merck chemicals. MeOH and EtOH solvents were used of AR grades.

Characterization techniques

Elemental analysis CHN was done using Elementar Vario EL III analyzer and the metal content in the complexes was determined using a thermoelectron IRIS INTREPID II XS PDUO ICP- AES instrument. MK-509 Digital conductivity meter was used to measure the conductance of the complexes at room temperature. The FT-IR spectra were recorded on a Thermo Nicolet Avatar370 spectrophotometer using KBr pellets in the 400-4000 cm^{-1} range. The UV-visible absorption spectra were recorded on a Varian Cray 500 UV-visible spectrometer.^{1}H NMR spectra were recorded using a Bruker-Avance III spectrometer with TMS as internal standard. Mass spectra of the compounds were obtained from Thermo Fischer Scientific Exactive HPLC PDA mass spectrometer using acetonitrile and MeOH as solvents.The magnetic measurements were carried out using Gouy's balance and diamagnetic corrections were carried out using Pascal's constant. The ESR spectrum of the Cu(II) complex was recorded in the solid-state at liquid nitrogen temperature (LNT) using a JES- FA200 ESR spectrometer. TGA analyses were recorded on a Simultaneous Thermal Analyser TG-DTA in the air with a heating range of 10-800 °C. Photocatalytic activities were investigated using Perkin Elmer Lambda 35 UV–Vis. Spectrophotometer. The high-resolution crystal structure of all the receptors for docking studies was downloaded from the RCSB protein data bank website. All MD calculations were performed on AutoDock 4.2 and AutoDock Vina.

Preparation of Schiff base

Indole-3-carboxaldehyde 2-aminobutyric acid (indal-2-abu)

2-abu (1.0312 g, 10 mmol) dissolved in EtOH (10 mL), was added slowly with constant stirring to an alcoholic solution (20 mL) containing KOH (0.5610 g, 10 mmol). The solution was magnetically stirred for 30 min and then filtered. To the filtrate indal (1.4516 g, 10 mmol) dissolved in EtOH (20 mL) was added dropwise with constant stirring and refluxed for 5 h. Two drops of conc. HCl was added to the above reaction mixture to remove potassium ions. The resulting solution was reduced to half of its original volume and kept at RT for one week. The yellow crystals obtained were recrystallized from MeOH. Scheme 1a shows the synthetic route of the Schiff base.

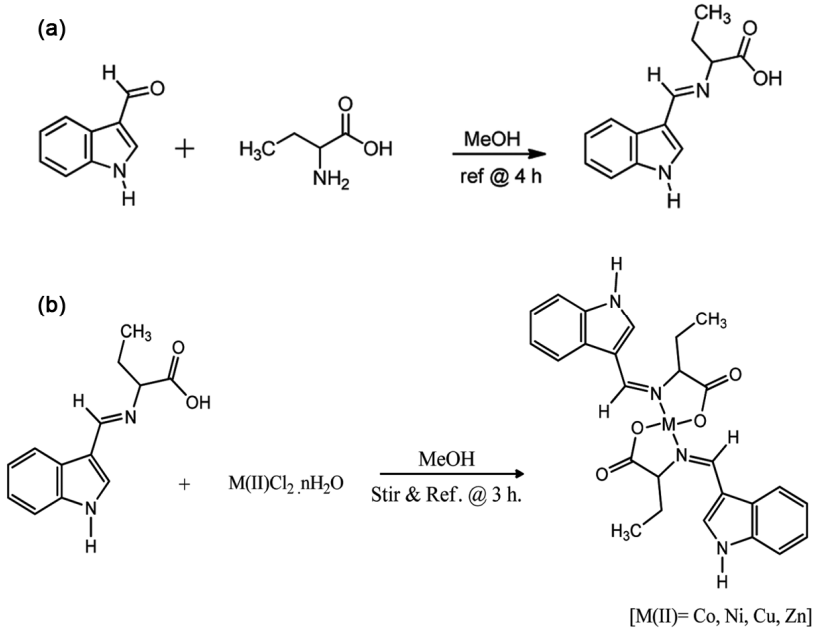

Scheme 1 — Synthetic route of (a) Schiff base and (b) metal complexes

Preparation of complexes

[Co/Ni/Cu/Zn(II)-(indal-2-abu)$_2$] complexes

A solution of cobalt chloride, nickel chloride, copper chloride and zinc chloride (5 mmol) in EtOH (15 mL) was slowly added to a solution of indal-2-abu (10 mmol) in MeOH (20 mL) and magnetically stirred. The above solution was stirred under reflux for 4 h resulting in the formation ofthe complex. The product thus obtained was filtered, washed several times with EtOH and finally dried in vacuum over anhydrous $CaCl_2$ and melting point was noted. The synthetic route for metal complexes is shown in Scheme 1b.

Molecular docking studies

All the MD calculations were performed on AutoDock4.2 and Auto Dock-Vina software. The original SB ligand, as well as H_2O molecules, were removed from the crystal structure, and polar hydrogens and united atom Kollman charges were assigned for the receptor using the graphical user interface ADT. The high-resolution crystal structure of corresponding receptors, 1,4-dihydroxy-2-naphthoyl-CoAsynthase (3T88), Alanine racemase (2RJG), DNA topoisomerase ATPase (3TTZ), β-alanine-pyruvate transaminase (3A8U), S. Aureus Dihydrofolate Reductase (3SRW) and Dihydro-pteroate synthase (2VEG), Mannotetraose 2-alpha-N-acetylglucosaminyl transferase (1QI3), Histidine ammonia-lyase (5X2L), Histidinol-phosphatase (3UGC), Histidine decarboxylase (1JS33) were acquired from the RCSB protein data bank.

Results and Discussion

Characterization of ligand

TLC technique was used for monitoring the reaction progress. The indal-2-abu is soluble in all common organic solvents such as EtOH, MeOH, but insoluble in water and has a yield of 83% and with a melting point of 260 ºC.

FT-IR spectrum

The IR spectrum of free SB (indal-2-abu) is shown in Supplementary Data, Fig. S1a, which revealed the absence of characteristic bands of the amino group of 2-abu and the carbonyl group of indal. The appearance of a new strong stretching frequency band that occurred at 1645 cm^{-1} is the characteristic of the azomethine group, confirms the formation of the proposed SB ligand[17]. The stretching frequency bands observed at 1632 and 1422 cm^{-1} in indal-2-abu could be ascribed to carboxyl asymmetric $\nu_{as}(COO^-)$ and symmetric $\nu_{sy}(COO^-)$ vibrations, respectively[18]. The IR spectrum of indal-2-abu also shows a broad band of medium intensity at 3436 cm^{-1} due to (NH) stretching and is superimposed with the strong band due to OH stretching vibration observed at 3282 cm^{-1}. The band observed at 1271 cm^{-1} in the SB ligand spectrum can be ascribed to ν(COO) carboxylic[19].

Mass spectrum

The mass spectrum of indal-2-abu exhibited a molecular ion peak at m/z 230.02, consistent with the molecular formula is depicted in Fig. 1a. The mass

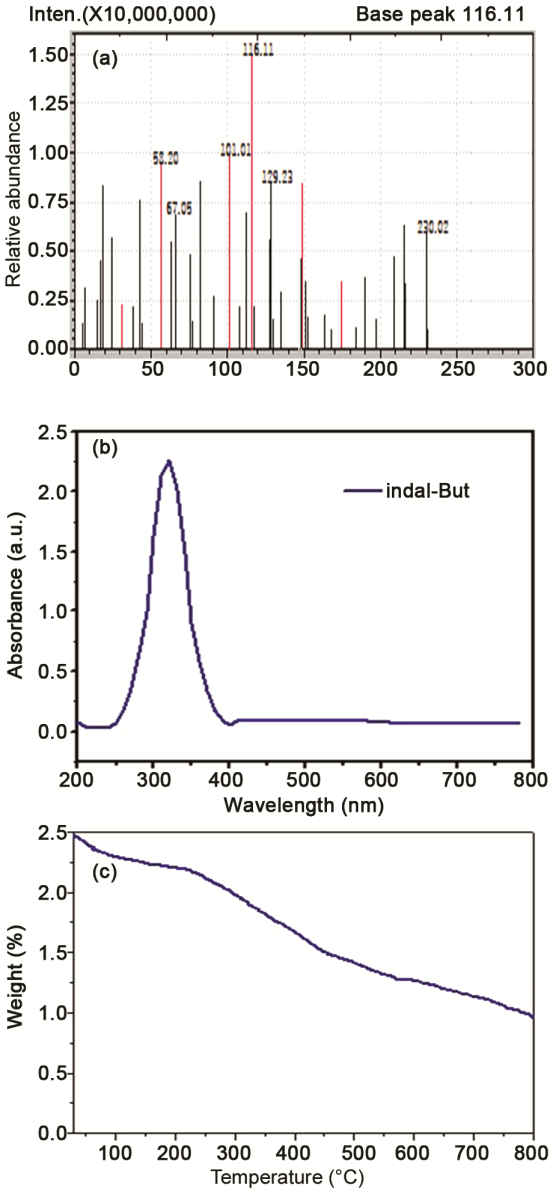

Fig. 1 — (a) Mass spectrum, (b) UV-visible spectrum and (c) TG curve of indal 2-abu

spectrum of indal-2-abu also exhibits a [M+1] peak at m/z 230.02. The base peak observed at m/z 116.11 corresponds to the fragment $[C_8H_6N]^+$. The different peaks that appeared in the mass spectrum of indal-2-abu are attributed to the fragmentation of the SB ligand molecule through the rupture of different bonds inside the molecule by successive degradation. The peaks that appeared at m/z 101.01 and 67.05 are respectively, corresponding to the fragments $[C_4H_7NO_2]$ and $[C_3H_3N_2]$.

Absorption spectrum

The UV-visible absorption spectrum of the SB indal-2-abu is shown in Fig. 1b. The spectrum exhibits an intense absorption band at 320 nm, attributed to π–π* transition of the C=N chromophore.

^{1}H NMR spectrum of ligand

The ^{1}H NMR spectrum of SB is demonstrated in Supplementary Data, Fig. S2a. In the spectrum of free SB ligand, the characteristic signal for aldehydic proton at δ 10.5 ppm was not observed, while a new singlet signal displayed at δ 8.28 ppm is assignable to azomethine proton[20], which confirms the formation of SB[20].

Thermal studies

The thermogram of indal-2-abu is clear evidence for the thermal stability of the compound up to 260 ^oC and the decomposition is a single step process is shown in Fig. 1c. The thermograms obtained for the sample is strong evidence for the absence of non-coordinated water molecules since they did not exhibit any endothermic peaks in the range 60-100 ^oC.

Molecular docking

The LGA was employed to calculate the energy between SB ligand and receptor[21,22]. The compound docked the active site of receptors with the grid centre dimension 40×40×40. The conformations with the lowest binding energy (BE) are extracted and analyzed in Discovery Studio Visualizer 4.0 software. The SB ligand (indal-2-abu) binds at the active site of the substrates by weak non-covalent interactions is presented in Fig. 2.

PASS prediction for the activity spectrum of indal-2-abuis tabulated in Supplementary Data, Table S1. The docked SB ligand forms a stable complex with the receptors depicted in Fig. 3. The BE values of the SB ligand with the substrate, 1 (3T88), (2RJG), (3TTZ), (3A8U), (3SRW) and (2VEG), (1QI3), (5X2L), (3UGC), (1JS33), are tabulated in Supplementary Data, Table S2. These preliminary results suggest that the compound has inhibitory activity against the receptors.

The (3T88), is a 6-chain structure with a sequence from "*bacillus coli*". It converts (OSB-CoA) to 1,4-dihydroxy-2-naphthoyl-CoA through an intra-molecular Claisen condensation in which the electrophile is an un-activated carboxylic acid. The active amino acid Thr117, Arg113 form conventional H-bond interaction with the N-atom, C=O bond, respectively having the distances 2.94, 2.95Å, whereas Asp110 has a carbon-H-bond with H(6) atom at the distance of 3.08 Å. Glu248, Asp110 forms electrostatic π-anion interaction with phenyl ring, pyrrole ring, respectively, showing the distances 4.91, 4.93Å. Arg113 form hydrophobic alkyl interaction with a CH_3 group and leu109 formulate hydrophobic π-alkyl interaction with phenyl ring are at the distances of 4.60, 4.63 Å, respectively.

The BE value of -6.9 MeV for 1,4-dihydroxy-2-naphthoyl-CoAsynthase-indal-2-abu complex provides important insight into the antibacterial property of the prepared compound. 2RJG is a four-chain structure with a sequence from *E. coli*, which catalyzesthe interconversion of L-alanine and D-alanine. It also provides the D-alanine required for cell wall biosynthesis.

Amino acids (Asn23, Ser27, Tyr43) forms conventional H-bond interaction with same C=O bond are at distances 2.30, 2.82, 2.07 Å whereas Ser45 shows conventional H-bond and C-H bond interactions with C-O group having the distances 3.00, 2.92 Å. Trp92, Trp108 displays two hydrophobic π-alkyl interfaces with CH_3 groups are at distances of 5.01, 4.64, 3.76, 3.96 Å. Leu110 shows two hydrophobic π-alkyl interactions with two ring centres are at distances 5.37, 4.96 Å while Ala50 has a hydrophobic π-alkyl interaction with phenyl ring centre at the distance of4.73 Å. The BE value of -7.7 MeV with indal-2-abu suggests the possible outcome of indal-2-abu based compounds as novel antibacterial agents.

(3TTZ), a double chain structure with the classification from *micrococcus-aureus* is an important enzyme across bacterial types and inhibition by antimicrobials effects in the interference of DNA synthesis and, subsequently, cell death. indal-2-abu interacts with 3TTZ through non-covalent interactions. Amino acids (Glu58, Arg84, Gly85) indicate conventional H-bond interaction with C-O

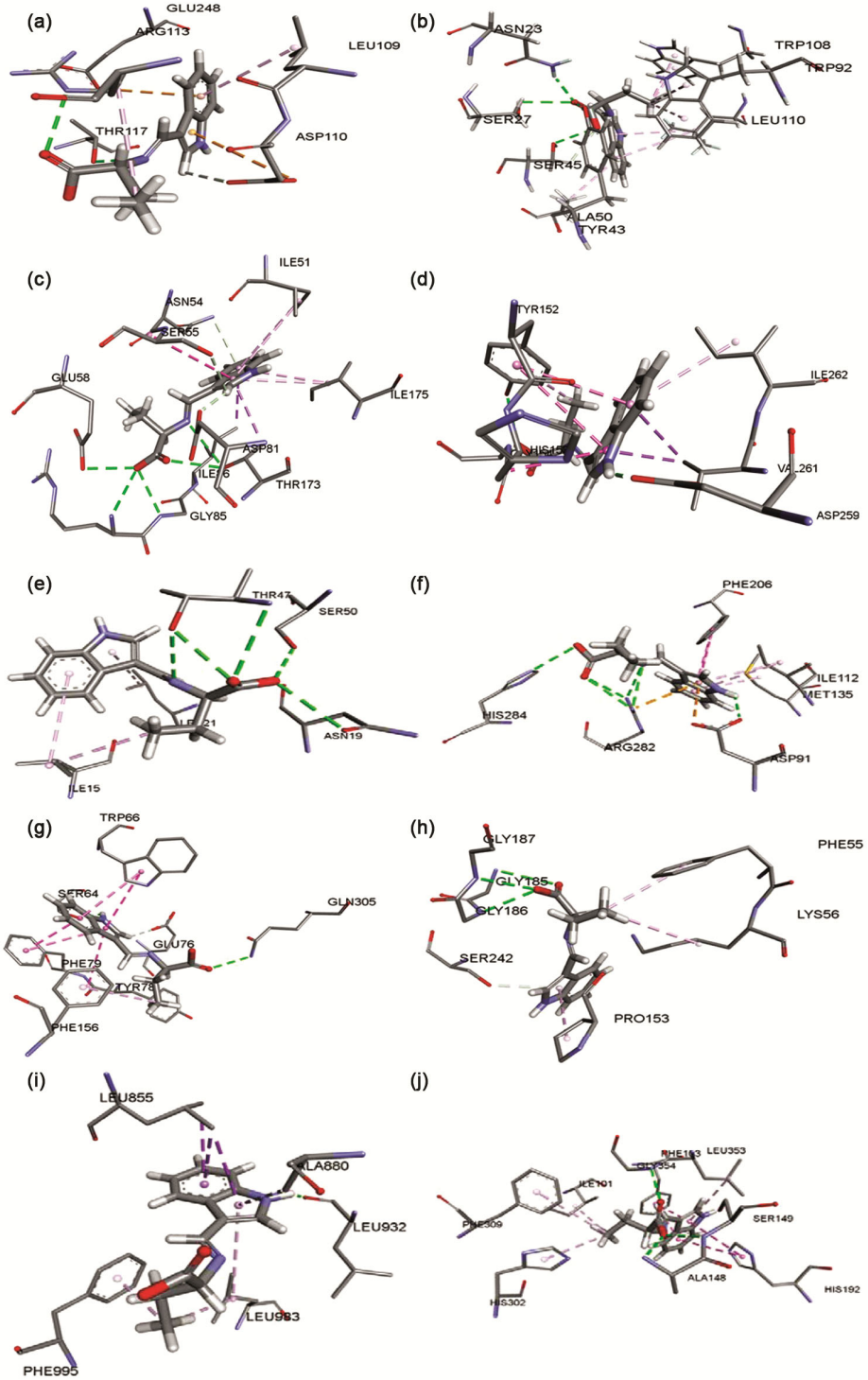

Fig. 2 — Interactive plot of amino acid residues of (a) (3T88), (b) (2RJG), (c) (3TTZ), (d) (3A8U), (e) (3SRW), (f) (2VEG), (g) (1QI3), (h) (5X2L), (i) (3UGC), and (j) (1JS33)

group at the distances of 2.85, 3.24, 2.88 Å while Thr173 shows two conventional H-bond interaction with C=O group and N-atom having the distances 3.334 and 3.09 Å.

Ser55, Asp81 shows C-H bond with H(6) atom and Asn54 has a C-H bond with pyrrole ring centre are at the distances of 2.79, 2.22, 3.49 Å. Ile86, Thr173 form hydrophobic π-σ interaction and Asn54 form

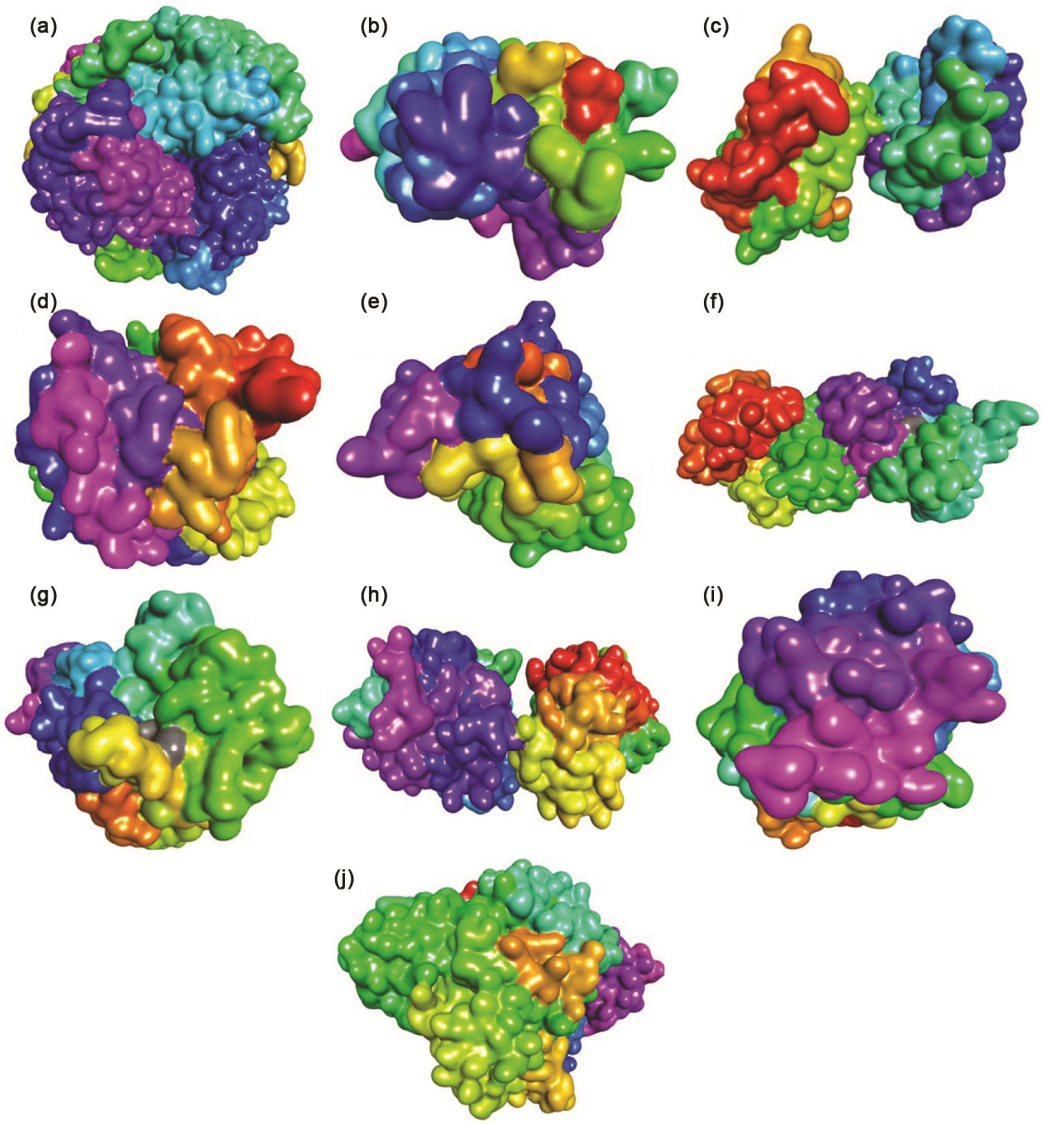

Fig. 3 — The docked ligand at the active site of (a) (3T88), (b) (2RJG), (c) (3TTZ), (d) (3A8U), (e) (3SRW), (f) (2VEG), (g) (1QI3), (h) (5X2L), (i) (3UGC), and (j) (1JS33)

amide-π-stacked interaction with pyrrole ring centre are at the distances of 3.94, 3.94, 5.08 Å, respectively. Ile51, Ile175 gives two hydrophobic π-alkyl interactions with centres of pyrrole ring and C_6H_5 ring are at the distances of 5.10, 5.45, 5.02, 5.13 Å. The BE value of -7.2 MeV with indal-2-abu shows that the inhibitor is a good applicant as an antibacterial agent.

3A8U is a single chain structure with a sequence from *bacillus-fluorescens-putidus*, which catalyzes transamination between a variety of omega-amino acids, mono and diamines, and pyruvate. Omega amino acids play an important role in metabolism. Hence, *β*-alanine-pyruvate transaminase inhibitors can effort as antibacterial agents. Amino acid Asp259 indicates conventional H-bond interaction with a H-atom involved to the pyrrole ring at the distances of 1.97 Å, while Tyr152, Gly154 forms conventional H-bond interaction with C-O bond at the distances 2.84, 3.51 Å.

Val261 shows two hydrophobic π-σ interactions and Tyr152 shows two hydrophobic π-π T-shaped interactions with centres of the phenyl ring and pyrrole ring are at the distances 3.79, 3.72, 4.88 and 5.13 Å. Ile262, Tyr152 formulates hydrophobic π-alkyl interaction with phenyl ring, methyl group are at the distances of 5.25 and 4.98 Å whereas His153 has a hydrophobic π-π T-shaped interaction with pyrrole ring at the distance of 4.10 Å. The BE value

of -7.1 MeV is obtained for indal-2-abu with *β*-alanine-pyruvate transaminase suggests the future possibility in the development of indal-2-abu based antimicrobial activities.

3SRW is a single chain structure with a sequence from *micrococcus-aureus* and is a key enzyme in folate metabolism. It catalyzes an essential reaction for de novo glycine and purine synthesis and for DNA precursor synthesis. Hence Dihydrofolate Reductase inhibitors (BE -7.5 MeV) provide a better candidate for antibacterial agents. indal-2-abu interacts with 3SRW through various non-covalent interactions as follows. The active amino acid Thr47 form two conventional H-bond interactions with C=O bond and a conventional H-bond interaction with nitrogen atom having the distances 3.20, 3.32, 2.87Å. Asn19, Ser50 forms conventional H-bond interaction with C-O bond at the distances of 2.99, 2.71 Å and Leu21 has a hydrophobic π-alkyl interaction with pyrrole ring at the distance of 5.20 Å. Ile15 form hydrophobic alkyl interaction with a CH_3 group and hydrophobic π-alkyl interaction with phenyl ring are at the distances 4.59, 5.00 Å.

2VEG catalyzes an essential step in the biosynthesis of folic acid and is the target for the sulphonamide group of antimicrobial drugs. The BE value of -6.2 MeV obtained for Dihydropteroate synthase- indal-2-abu reveals that indal-2-abu based compounds are better candidates as Dihydrofolate Reductase inhibitors. The active amino acid Arg282 forms two conventional H-bond interactions with C=O groups and two conventional H-bond interactions with the same nitrogen atom are at the distances of 3.29, 3.24, 3.08, 3.23 Å. Asp91 has a conventional H-bond interaction with the H-atom attached to the pyrrole ring and His248 forms a conventional H-bond interaction with the C-O group are at the distances of 2.36, 3.13 Å, respectively. Arg282 show an electrostatic π-cation interaction and Asp91 show an electrostatic π-anion interaction with the pyrrole ring at the distances of 4.17, 3.74 Å. Phe206 gives two hydrophobic π-π T-shaped interactions with centres of phenyl ring and pyrrole ring are at the distances 5.11, 5.22 Å. Met135, Ile112 shows hydrophobic π-alkyl interaction with phenyl ring having the distances 5.13, 4.44 Å while Ile112 shows hydrophobic π-alkyl interaction with pyrrole ring at a distance 5.35 Å.

1QI3 is a single chain structure with a sequence from *Achromobacter sewerinii* whose amino acid residues are involved in the intermediate formation in the hydrolysis reactions. The residue Ser64 show conventional H-bond interaction with a H-atom attached to the pyrrole ring at the distances of 2.16 Å whereas Gln305 form conventional H-bond interaction with C=O group at the distances of 2.49 Å. Glu76 has a C-H bond with H(6) atom and Tyr78 shows an amide-π-stacked interaction with pyrrole ring are at the distances of 2.68, 4.97 Å, respectively. Phe79 indicates two π-π-stacked interactions and Trp66 forms two hydrophobic π-π T-shaped interactions with two ring centres are at distances of 3.98, 5.05, 4.77, 5.06 Å. Tyr78, Phe156 formulates hydrophobic π-alkyl interaction with CH_3 group showing the distances 5.04, 5.22 Å.

(5X2L) catalyzes the synthesis of D-serine from L-serine[23]. Most of the endogenous free d-serine (~90%) in the brain is produced by serine racemase. d-Serine in the brain is involved in neurodegenerative disorders and epileptic states. Thus, serine racemase inhibitors are expected to be novel therapeutic candidates for the treatment of these disorders[24]. The SB ligand (indal-2-abu) binds at the active site of 5X2L by weak non-covalent interactions. Amino acids Gly186, Gly187 form conventional H-bond interaction with C-O bond and Gly185 form conventional H-bond interaction with C=O bond are at the distances of 2.83, 2.95, 3.17Å,respectively. Ser242 shows π-donor H-bond and Pro153 have a hydrophobic π-alkyl interaction with pyrrole ring having the distances 3.49, 4.90 Å. Lys56 indicates hydrophobic alkyl interaction and Phe55 has a hydrophobic π-alkyl interaction with methyl group are at the distances of 5.12, 4.82Å. The BE value of -6.8 MeV for indal-2-abu towards the target enzyme 5X2L thus provides a molecular basis for the development of such novel therapeutic compounds.

3UGC is a single chain structure with a sequence from the human. 3UGC is involved in various processes such as cell growth, development, differentiation, or histone modifications as these enzymes are responsible for the activation of many proteins by adding a phosphate group to the protein. 3UGC inhibitors normally work by inhibiting this phosphorylation process. For the treatment of rheumatoid arthritis, psoriasis, myeloproliferative neoplasms, and leukem[25,26] so kinase inhibitors are actuality developed.

Indal-2-abu binds at the active site of 3UGC through different types of weak non-covalent

interactions as follows. The active amino acid Leu855 shows two hydrophobic π-σ interactions with phenyl ring centre and a hydrophobic π-sigma interaction with pyrrole ring centre having distances 3.73, 3.82, 3.91 Å. Leu932 form a conventional H-bond interaction with a H-atom attached to the pyrrole ring showing the distance 2.38 Å while Leu983, Phe995 gives hydrophobic π-alkyl interaction with a methyl group at the distances of 5.31, 3.89 Å.

Leu983 has a hydrophobic alkyl interaction and Ala880 has a hydrophobic π-alkyl interaction with the pyrrole ring centre at the distances of 4.92, 4.83 Å, respectively. The BE value of -8.0 MeV for indal-2-abu with (3UGC) could throw light on its inhibitory activity against leukemia, rheumatoid arthritis, psoriasis, *etc.* 1JS33, is a double chain structure responsible for the synthesis of the key neuro-transmitters dopamine and serotonin *via* decarboxylation of L-3,4-dihydroxyphenylalanine and L-5-hydroxytryptophan, respectively[27]. DOPA decarboxylase has been implicated in a number of clinical disorders, including Parkinson's disease and hypertension.

The amino acids (Ala148 and Ser149) forms conventional H-bond interaction with C-O group and Gly354 forms a conventional H-bond interaction with C=O group are at distances 3.16, 2.98, 2.97 Å. Phe103 formulates two π-π-stacked interactions and His192 forms two hydrophobic π-π T-shaped interactions with two ring centres are at distances of 3.83, 3.84, 4.73, 5.41 Å, respectively.

His302, Phe309 gives hydrophobic π-alkyl interaction with methyl group showing the distances 4.51, 4.88 Å. Ile101 has a hydrophobic alkyl interaction with a methyl group and Leu353 show a hydrophobic π-alkyl interaction with the pyrrole ring are at the distances 4.18, 5.01 Å. The structure of the 1JS3 doped with indal-2-abu with binding energy -8.3 hence provides the molecular basis for the development of new inhibitors of Dopa decarboxylase with good pharmacological effects[26]. Based on the structure of a compound, PASS analysis[28]was done, which predicts different types of activities and is listed in Supplementary Data,Table S3.

Characterization of complexes

All the metal complexes are stable at room temperature, soluble in some organic solvents such as MeOH, DMF and DMSO. All the complexes have a yield of 78-72%, and their melting points fall in the range ~315-320ºC. The analytical data of [Co-(indal-2-abu)$_2$],[Ni-(indal-2-abu)$_2$], [Cu-(indal-2-abu)$_2$], and [Zn-(indal-2-abu)$_2$] complexes are depicted in Table 1. Analytical data agrees well with the molecular formula assigned for indal-2-abu and its complexes.Moreover, all the metal complexes have 1:2 metal to ligand (ML_2) stoichiometry.

Molar conductance

The molar conductance data of [Co-(indal-2-abu)$_2$],[Ni-(indal-2-abu)$_2$], [Cu-(indal-2-abu)$_2$], and [Zn-(indal-2-abu)$_2$] complexes are provided in Table 1. Conductivity measurements were carried out on 10^{-3} M solution for all metal complexes in MeOH medium as solvent. The low molar conductivity values that fall in the range of 9-12 $\Omega^{-1}cm^2mol^{-1}$ suggest non-electrolytic behaviour[29] for the metal complexes.

FT-IR spectra

The IR spectra of [Co-(indal-2-abu)$_2$], [Ni-(indal-2-abu)$_2$], [Cu-(indal-2-abu)$_2$], and [Zn-(indal-2-abu)$_2$] are depicted in Supplementary Data, Fig. S1b-e. The IR spectrum of the free indal-2-abu exhibited a band at 1645 cm^{-1} is attributed to azomethine group vibration. This band was shifted to lower frequency regions from 1630, 1621, 1631, 1629 cm^{-1}, respectively, suggesting the coordination of azomethine nitrogen with the metal ion. This is further substantiated by the presence of a new band at 420-450 cm^{-1} assignable to υ(M-N) stretching frequency bands[30]. The band due to O–H stretching disappeared in the spectrum of complexes and lower shifting were observed for the carboxyl asymmetric $\nu_{as}(COO^-)$ and symmetric $\nu_{sy}(COO^-)$ stretching bands at 1620-1640 and 1418-1446 cm^{-1}, respectively, during complexation indicate the linkage between metal ions and carboxylate oxygen atom after deprotonation. The magnitude of separation of these stretching frequencies between $\nu_{as}(COO^-)$ and $\nu_{sy}(COO^-)$ vibrations was found to be 194-207 cm^{-1} in the complexes suggests the unidentate binding fashion

Table 1 — Analytical data of indal-2-abu and its complexes

Complexes	λ_{max} (nm)	Transitions	Geometry
[Co-(indal-2-abu)$_2$]	560	$^4A_2$ (F)→$^4T_1$(F)	Tetrahedral
[Ni-(indal-2-abu)$_2$]	630	$^3T_1$→$^3T_1$(P)	Tetrahedral
[Cu-(indal-2-abu)$_2$]	640	^2B_1g → ^2A_1g	Square planar
[Zn-(indal-2-abu)$_2$]	450	LMCT	Tetrahedral

Calculated values are given in parenthesis

of carboxylate oxygen atom with the metal ion[31,32]. The position of the N–H band did not show any considerable change from that of the free ligand, indicating that nitrogen of NH group of indal is not involved in coordination with the metal. A weak band that appeared at 519-570 cm^{-1} is assigned to ν(M-O) vibration[33].Thus from the above discussion, it may be concluded that indal-2-abu behaves as a bidentate SB ligand coordinated to the metal ion *via* oxygen atom of the carboxyl group of 2-abu and nitrogen atoms of the imine groups of azomethine linkage. Some important selected IR spectral bands of indal-2-abu and its complexes are shown in Table 2.

^{1}H NMR spectrum

In the spectrum of [Zn-(indal-2-abu)$_2$] complex is shown in Supplementary Data, Fig. S2b. The azomethine proton upon coordination displayed a downfield shift and the chemical shift value increased to 9.00 ppm. This shift to a higher δ value confirms the coordination of azomethine nitrogen with the metal. The signal corresponding to 8.25 ppm in the spectrum of indal-2-abu and 8.09 to 8.40 ppm in the spectrum of [Zn-(indal-2-abu)$_2$] complex corresponds to indole-transene proton. The multiplet signals were seen in the spectrum fall in the range 7.21 to 7.53 ppm in the spectrum of indal-2-abu can be attributed to aryl CH protons.The indal-2-abu also gave a signal at 9.95 ppm assignable to COOH proton. The absence of this signal in the spectrum of [Zn-(indal-2-abu)$_2$] complex suggests the participation of COOH moiety in chelation after deprotonation. Thus, the ^{1}H NMR spectral data further substantiates the mode of chelation is provided by IR spectral data.

Mass spectra

The mass spectra of [Co-(indal-2-abu)$_2$],[Ni-(indal-2-abu)$_2$], [Cu-(indal-2-abu)$_2$], and [Zn-(indal-2-abu)$_2$] complexes exhibited a molecular ion peak at m/z 517.12, 517.05,522.01 and 523.54, respectively, consistent with the proposed molecular formula and confirms 1:2 metal to ligand ratio.

In the cobalt complex, the peak observed at m/z 185 may be assigned to the fragment [$C_{12}H_{13}N_2$] formed due to removal of [CO_2•] from the first fragment [$C_{13}H_{13}N_2O_2$] after the cleavage of M-O and M-N bonds. The mass spectrum also displayed an [M+1] peak at m/z 518.20.The LC-MS spectrum obtained for [Ni-(indal-2-abu)$_2$] complex the base peak was observed at m/z 114.05 can be assigned to the fragment [C_8H_7N].

The mass spectrum of [Cu-(indal-2-abu)$_2$] is shown in Fig. 4.The mass spectrum of the copper complex also displayed low intensity [M +2] and [M +3] peaks. The base peak was observed at m/z 114.12 and can be attributed to the fragment [$C_5H_8NO_2$].The peaks observed at m/z 117.01 can be ascribed to the formation of the fragment [C_8H_7N] through α-cleavage. As expected, the mass spectrum of the zinc complex also displayed a base peak observed at m/z 117.21 is ascribed to the formation of the fragment [C_8H_7N]. The peaks observed from the spectrum support the structure and stoichiometry ratio of the complex.

Absorption spectra

The absorption spectral measurements were used for assigning the geometry of complexes based on the positions and number of d–d transition peaks[34]. The

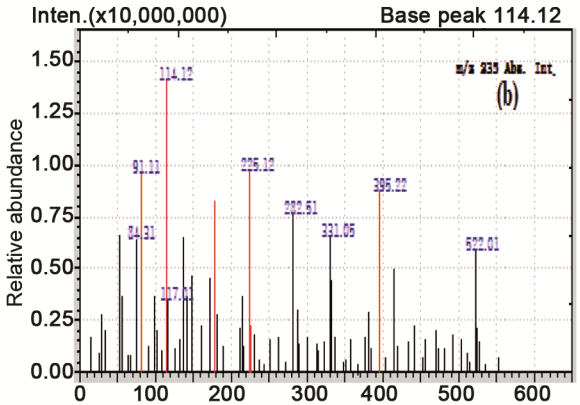

Fig. 4 — Mass spectrum of [Cu-(indal-2-abu)$_2$]

Table 2 — Important IR spectral bands of indal-2-abu and its complexes

Ligand/Complex	IR bands, wavenumber (cm^{-1})						
	ν(C=N)	$\upsilon_{as}(COO^-)$	$\upsilon_{sy}(COO^-)$	Δ(COO^-)	ν(N-H)	ν(M-O)	ν(M-N)
indal-2-abu	1645	1632	1422	210	3436	-	-
[Co-(indal-2-abu)$_2$]	1630	1640	1446	194	3430	519	420
[Ni-(indal-2-abu)$_2$]	1621	1620	1418	202	3432	542	448
[Cu-(indal-2-abu)$_2$]	1618	1620	1422	198	3436	560	462
[Zn-(indal-2-abu)$_2$]	1629	1627	1420	207	3430	570	459

electronic spectrum of [Co-(indal-2-abu)$_2$] complex exhibited a single absorption band in the visible region at 560 nm, which is due to $^4A_2(F)\rightarrow{}^4T_1(F)$ transition. This value favours tetrahedral geometry for the complex[35]. The electronic spectrum of nickel complex shows two d-d transition bands at 630 and 310 nm, assignable $^3T_1\rightarrow{}^3T_1(P)$ and LMCT transitions, respectively, indicating tetrahedral geometry for this complex[36]. In general, due to Jahn–Teller distortion, copper complexes provide a broad absorption band between 600 and 700 nm for a square planar environment. For the [Cu-(indal-2-abu)$_2$] complex, broadband was observed at 640 nm and can be assigned to $^2B_1g \rightarrow {}^2A_1g$ indicates the square planar geometry of the copper complexes[37]. The electronic spectrum of [Zn-(indal-2-abu)$_2$] complex exhibited an absorption band at 450 nm attributed to LMCT transition resulting intense bands, which is well-suited with tetrahedral geometry for this complex. Important electronic spectral data assignments of metal complexes are listed in Table 3 and its spectra are shown in Fig. 5.

Magnetic measurements

Magnetic susceptibility data of [Co-(indal-2-abu)$_2$],[Ni-(indal-2-abu)$_2$], and [Cu-(indal-2-abu)$_2$] complexes are tabulated in Supplementary Data, Table S4. The observed deviation of magnetic moment values for metal ions in the complex from the theoretical spin only values for free metal ions is because of the presence of the external ligand field. Diamagnetic corrections are corrected and applied

Table 3 — Electronic spectral data of metal complexes

Complexes	λ_{max} (nm)	Transitions	Geometry
[Co-(indal-2-abu)$_2$]	560	$^4A_2$ (F)$\rightarrow{}^4T_1$(F)	Tetrahedral
[Ni-(indal-2-abu)$_2$]	630	$^3T_1\rightarrow{}^3T_1$(P)	Tetrahedral
[Cu-(indal-2-abu)$_2$]	640	$^2B_1g \rightarrow {}^2A_1g$	Square planar
[Zn-(indal-2-abu)$_2$]	450	LMCT	Tetrahedral

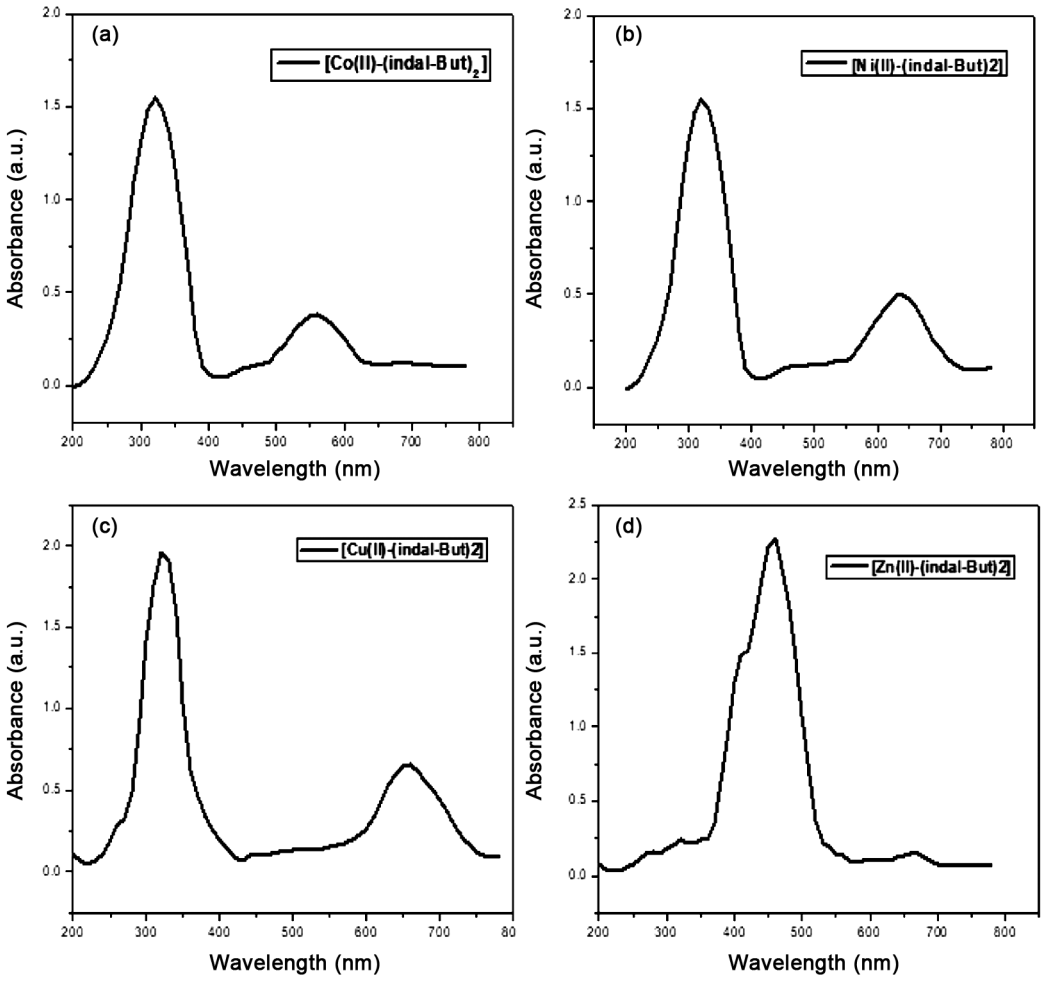

Fig. 5 — Electronic spectra of (a) [Co-(indal-2-abu)$_2$], (b) [Ni-(indal-2-abu)$_2$], (c) [Cu-(indal-2-abu)$_2$] and (d) [Zn-(indal-2-abu)$_2$]

during the measurement of magnetic susceptibility because the presence of inner core electrons, ligand field, atoms and ions in the material *etc*. will make the apparent molar susceptibility smaller than it really is from the contribution of unpaired electrons.

The observed effective magnetic moment of 3.95 BM corresponded to [Co-(indal-2-abu)$_2$] complex and was greater than the spin-only value of 3.87 BM for tetrahedral geometry. The larger value of μ_{eff} obtained than the calculated value may be attributed to spin-orbit coupling.The [Ni-(indal-2-abu)$_2$] was found to have an effective magnetic moment of 3.51 BM and hence it favours tetrahedral geometry. Here also, the observed effective magnetic moment is found to be higher than the spin-only value due to spin-orbit coupling. The observed magnetic moment value of 1.82 BM for the [Cu-(indal-2-abu)$_2$] suggests a square planar field around the metal ion. Electronic spectral data and magnetic moment data favours a square planar environment for this complex.The [Zn-(indal-2-abu)$_2$] is found to be diamagnetic and it would have tetrahedral geometry.

ESR spectrum

The ESR spectrum of a powdered sample of [Cu-(indal-2-abu)$_2$] complex is given in Supplementary Data, Fig. S4, measured at LNT showed characteristic signals with $g_{\|}$ = 2.114 and $g_{\perp}$= 2.053. The trend $g_{\|}>g_{\perp}>2$ indicating that the unpaired electron lies in the $_x^2$-$_y^2$ orbital[38] , characteristic of square planar geometry around the copper ion. For square planar geometry, the ground state is the $d_{x^2-y^2}$ orbital and the $g_{\|}$ and $g_{\perp}$ values could be found out using the following equation.

$$g_{\|}= g_z= 2.0023 \pm 8\,{}^{\lambda}/_{E}(dx^2\text{-}y^2)\text{-}E(d_{xy})$$
$$g_{\perp} = g_x = g_y = 2.0023 \pm 2\,{}^{\lambda}/_{E}(d_x{}^2\text{-}_y{}^2)\text{-}E(d_{xz})$$
or
$$g_{\perp} = g_x = g_y = 2.0023 \pm 2\,{}^{\lambda}/_{E}(d_x{}^2\text{-}_y{}^2)\text{-}E(d_{yz})$$

where λ is the spin–orbit coupling, constant for copper ion and E are the orbital energies. The nuclear quantum number of copper is $^3/_2$; hence it should show four signals in the spectrum corresponding to the coupling of the electron spin of^{63}Cu nucleus (I = $^3/_2$).However, all the signals are not observed in the complex.

The $g_{\|}$ and $g_{\perp}$ values depart considerably from the free ion value and the shifting of g value for hyperfine splitting is indicative of the nature of bonding. If the g-value shows a negative shift with respect to the free-electron g-value (2.0023),the bonding is ionic and if the shift is positive, then the bond will be more covalent in nature. The shifting of g-values from 2.0023 in transition metal complexes is due to mixing *via* spin-orbit coupling of the metal orbitals containing the unpaired electron(s) with the empty or filled ligand orbitals[39]. When the metal orbitals mix with empty ligand orbitals, there occurs a negative g shift, whereas a positive shift in g value can be observed when the mixing is with the filled ligand orbitals.

Moreover, the extent of shift depends on the amount of unpaired electron density at the donor sites of the ligands, which again is a direct measure of the degree of covalency of the complex. The ESR spectrum of the [Cu-(indal-2-abu)$_2$] complex shows splitting in the $g_{\|}$ region. Hence $g_{\|}$ value can be used as a measure of the nature of the metal-ligand bond[40].Accordingly, for ionic environment, the value should be more than 2.3 and if it is less than 2.3 it corresponds to covalent nature. Since $g_{\|}$ value for the [Cu-(indal-2-abu)$_2$] complex is less than 2.3 it confirms the covalent character of the metal-ligand bond.It is also reported that $g_{\|} > 2.4$ in complexes corresponds to Cu-O bonds and $g_{\|}> 2.3$ corresponds to Cu-N bonds[41,9]. Hence the observed $g_{\|}$ value of 2.114 for [Cu-(indal-2-abu)$_2$] can be ascribed to the presence of mixed Cu-O and Cu–N bonds. The nature of the ligand forming the complex is evaluated from the exchange interaction parameter term *g. The g*-value can be calculated using the formula $G = (g_{\|}\text{-}2.0023)/(g_{\perp}\text{-}2.0023)$. If $\boldsymbol{G} < 4.0$, the ligand field is considered strong. For the square planar complexes[42] the *g*-value is usually in the range of 2.03–2.45. Since the *g*-value obtained for the copper complex is 2.203 at LNT, it suggests that the indal-2-abu provides a sufficiently strong field in [Cu-(indal-2-abu)$_2$] complex.

Thermal studies

The thermogram of metal complexes did not exhibit any weight loss up to 250-290 ºC, suggesting stability and the absence of water molecules in the complexes. In the complexes from the thermogram, it was noticed that the first stage of thermal decomposition noticed in the temperature range of 250-350 ºC corresponding weight loss of 22.3-28 % may be attributed due to the melting and partial decomposition of indal-2-abu. The resultant complexes then exhibited a weight loss of 30-40%, also exhibiting the second stage of decomposition

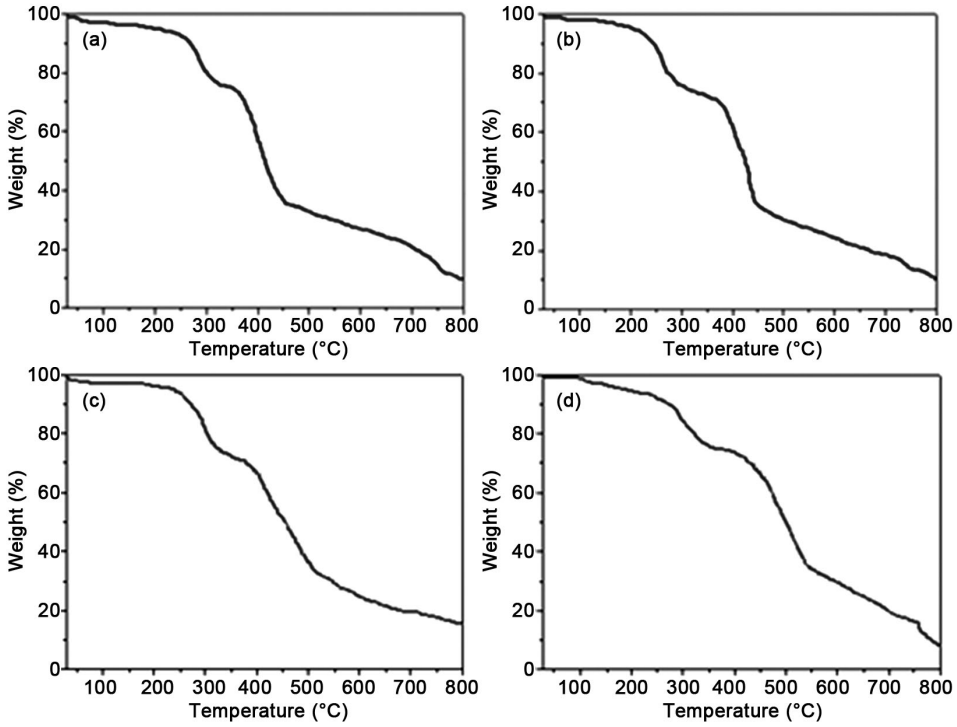

Fig. 6 — TG curves of (a) [Co-(indal-2-abu)$_2$], (b) [Ni-(indal-2-abu)$_2$], (c) [Cu-(indal-2-abu)$_2$]

ranges from 380-550 ºC. After the complete decomposition, the minimum mass loss of 7.2 to 7.5% was observed after 750 °C due to the metal oxide residue in the complexes. The inflation of the TGA curve of the complex at a temperature below 750-800 °C indicates the decomposition of the fully organic part of the chelate, leaving the metallic oxide at the final temperature.TG curves of (a) [Co-(indal-2-abu)$_2$], (b) [Ni-(indal-2-abu)$_2$] and,(c) [Cu-(indal-2-abu)$_2$]are shown in Fig. 6.

Magnetic susceptibility data together with electronic and EPR spectral data are sufficient to confirm the geometry of complexes. The proposed structure of the SB ligand and its complexes are shown in Fig. 7.

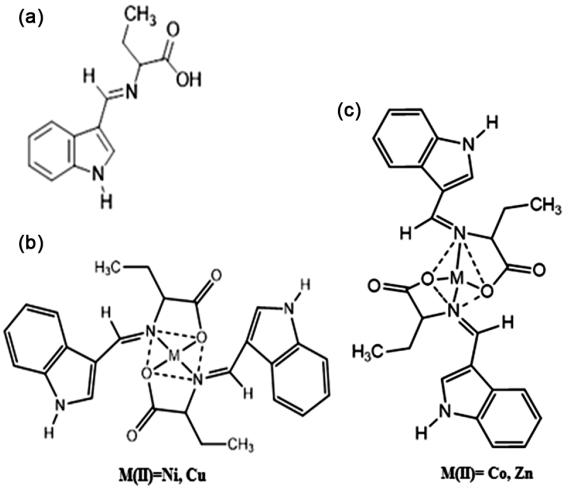

Fig. 7 — Proposed structure of (a) indal-2-abu, (b) optimized structure of indal-2-abu, (c) [Co-(indal-2-abu)$_2$], (d) [Ni-(indal-2-abu)$_2$], (e) [Cu-(indal-2-abu)$_2$], and (f) [Zn-(indal-2-abu)$_2$]

Photocatalytic studies

The photocatalytic dye degradation efficiencies of indal-2-abu, [Co-(indal-2-abu)$_2$], [Ni-(indal-2-abu)$_2$], [Cu-(indal-2-abu)$_2$] and[Zn-(indal-2-abu)$_2$] complexes were studied by the degradation of MB are depicted in Fig. 8. The photocatalytic degradation was measured both before and after exposure to sunlight irradiation on the mixture with and without using a catalyst. A series of concentrations of 5, 10, 15 and 20 mg of the prepared catalyst were mixed in a 100 mL aqueous solution of MB (10 mg/1000 mL). The suspension thus obtained was then allowed to react in the presence of sunlight under constant stirring. After irradiation, the catalyst was separated by centrifugation and the absorbance of MB was measured at 664 nm in the remaining dye during the photo-degradation. The percentage of dye degradation was calculated using the following formula

$$\% \text{ of MB degradation} = \left(\frac{c_0 - c}{c_0}\right) \times 100$$

Where C_0 is the initial concentration of MB solution before the photocatalytic reaction and C is the concentration of MB solution after the photocatalytic reaction. There was no appreciable degradation with catalyst without irradiation. Therefore, sunlight irradiation was necessary for effective degradation. The photocatalytic degradation also depends on the amount of catalyst, *i.e.,* an increase in the number of active sites on the catalytic surface increases the degradation[43].The effect of irradiation time on the photocatalytic degradation of MB was studied at different time intervals from 0 to 120 min. with MB concentration of 10 mg/L, at neutral pH. Percentage degradation of MB with time is given in Supplementary Data, Table S5, and the time-dependent degradation efficiency of the catalyst is depicted in Fig. 8f.

It is noticeable that for all five catalysts, the maximum degradation efficiency was observed in 90 min. with degradation of 63.15, 85.28, 80.10, 84.23 and 78.12%, respectively for indal-2-abu,[Co-(indal-2-abu)$_2$] ,[Ni-(indal-2-abu)$_2$], [Cu-(indal-2-abu)$_2$], and [Zn-(indal-2-abu)$_2$] complexes on irradiation of sunlight. The highest degradation (85.28%) was observed for the catalyst [Co-(indal-2-abu)$_2$] complex at 90 min. irradiation. The efficiency of degradation of MB was found to be decreased on further increase in irradiation time.

The decrease in degradation efficiency after 90 min. can be explained on the basis of the general fact

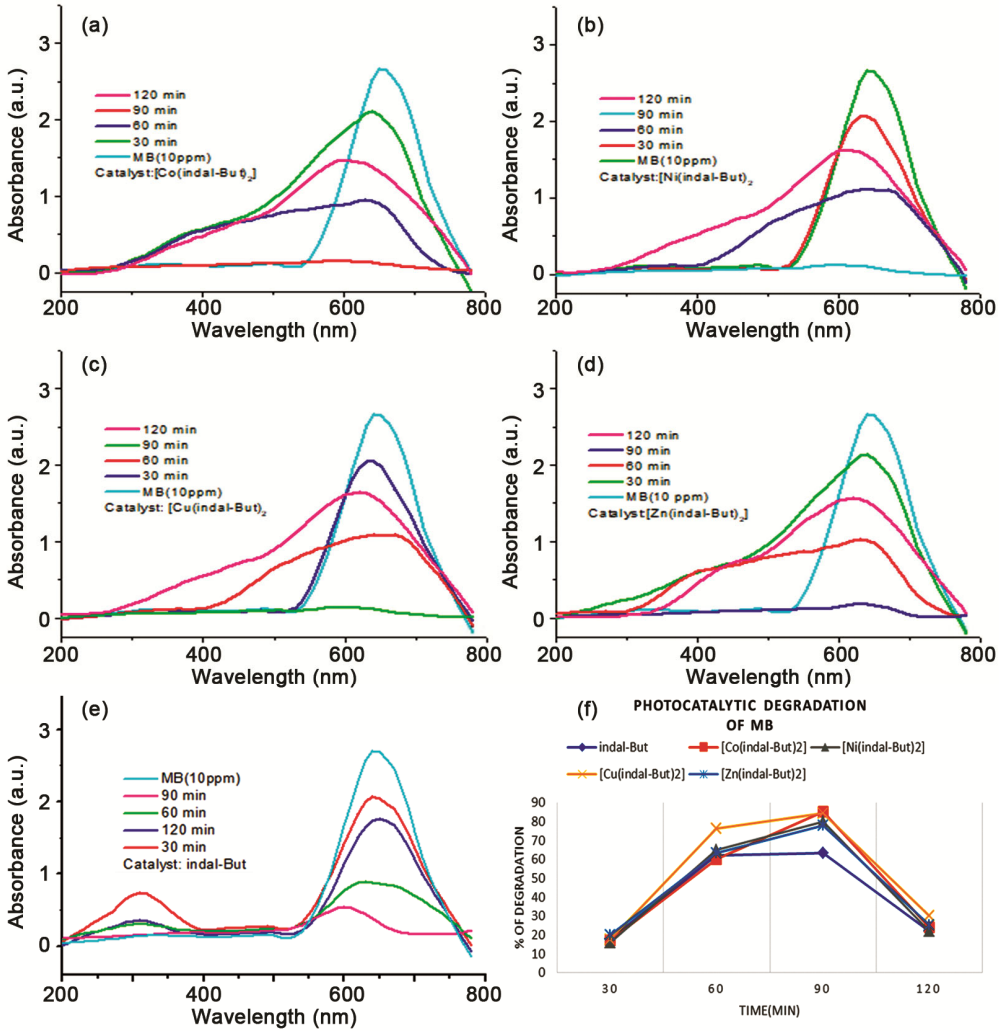

Fig. 8— Photocatalytic degradation of MB with respect to time using (a) [Co-(indal-2-abu)$_2$], (b) [Ni-(indal-2-abu)$_2$], (c) [Cu-(indal-2-abu)$_2$], and (d) [Zn-(indal-2-abu)$_2$], (e) indal-2-abu as catalyst and (f) degradation (%) of MB with time for metal complexes ((a) indal-2-abu, (b) [Co-(indal-2-abu)$_2$], (c) [Ni-(indal-2-abu)$_2$], (d) [Cu-(indal-2-abu)$_2$] and, (e) [Zn-(indal-2-abu)$_2$])

that there is a possibility of recombination of charge carriers and also the desorption process of adsorbed reactant species[44]. A tentative mechanism has been proposed on the basis of the experimental observations and the literature reports, as follows. When the metal complex is irradiated with sunlight, it absorbs photons and then charge separation occurs at the interface and promoting the photocatalytic activity of the photocatalyst.

Sunlight radiation interacts with MB dye molecules, and this interaction results in producing of excited dye molecules. Then the excited dye molecules react with oxygen to give a positive radical of dye and a negative radical of oxygen. Afterward, the negative radical interacts with H^+ ions liberated from water to produce superoxide radicals ($OOH^·$) responsible for the degradation of the dye molecule[19].

The photogenerated holes, reducing their recombination with the electrons, and the surface of OH groups allow the adsorption of O_2 from water. Then, the photo-formed electrons reduce O_2 to O_2^- species, which may interact with water to form further oxygenated radicals, mainly hydroxyl radicals. Both hydroxideand superoxide radicals will effectively increase the rate of dye molecule degradation, and thus MB dye decolorises effectively[19].

Microbiological studies

The gram-positive bacterial species *Bacillus subtilis (B. subtilis*) and *Staphylococcus aureus (S. aureus*), and gram-negative bacterial species *Pseudomonas aeruginosa (P. aeruginosa*) and *Escherichia coli (E. coli)* were chosen to examine the antibacterial property of the prepared compounds by disk diffusion technique using a nutrient agar medium[25,45]. The antifungal activities of the compounds were also tested against *Aspergillus niger (A. niger*) and *Candida albicans (C. albicans*) using Potato dextrose agar medium[46,47].

In this method, the agar plates are inoculated with a standardized inoculum of the test microorganism. Then, filter paper discs (about 6 mm in diameter), containing the test compound at the desired concentration are placed on the agar surface. The Petri dishes are incubated under suitable conditions. Generally, antimicrobial agent diffuses into the agar and inhibits germination and growth of the test microorganism and then the diameters of inhibition growth zones were measuredas millimetres (mm) and MIC were calculated and compared with the standards, Ciprofloxacin, and Fluconazole drugs.

Most of the complexes show excellent activity against gram-negative bacteria *E. coli* and the promising activity of these compounds against gram-negative bacteria throws light to the possible future of these compounds as antitumour agents since gram-negative bacteria are considered as quantitative microbiological methods for testing beneficial and important drugs in both clinical and experimental tumour chemotherapy.

Among the metal complexes, [Cu-(indal-2-abu)$_2$] shows the maximum activity and its activity is even higher than the standard drug ciprofloxacin against two organisms and shows comparable activity to that of fluconazole against two organisms. This can be explained based on the chelation effect, which can inhibit the role of metal dependant proteins by disturbing the microbial cell homeostasis and culminating in the blockage of microbial nutrition, growth and development[48].

The highest antifungal activity was obtained for [Co-(indal-2-abu)$_2$] against *A. Niger* with an MIC value of 18 μg mL^{-1}. The [Ni-(indal-2-abu)$_2$] complex showed an MIC value of 17 and 18 μg mL^{-1} respectively, against *E. coli* and *S. aureus*and the result was comparable to the activity of standard drug Ciprofloxacin. The *in vitro* antibacterial activity results revealed that the highest activity is expressed by [Zn-(indal-2-abu)$_2$] against *E. coli,* and *B. subtilis* with an MIC value of 16 μg mL^{-1}. The [Zn-(indal-2-abu)$_2$] was also found to be effective against *A. niger* and *C. albicans* with MIC values are 19 and 20 μg mL^{-1}, respectively. The MIC data of synthesized compounds against tested microorganisms are given in Supplementary Data, Table S6. A bar diagram representing the growth of inhibition zones was measured and the metal complexes exhibit higher activity than the SB against all organisms, as given in Fig. 9.

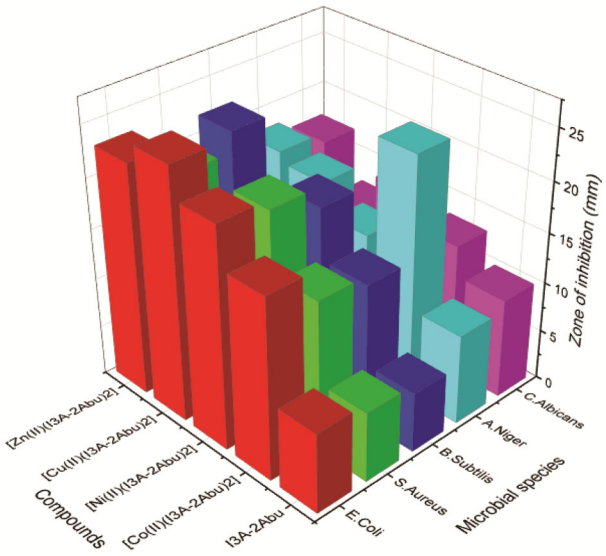

Fig. 9 — The antimicrobial activity of indal-2-abu and its metal complexes

Conclusions

The spectroscopic studies, along with thermal and magnetic moment data favours tetrahedral geometries for Co(II), Ni(II) and Zn(II) complexes while a square planar geometrical environment for the copper complex. Among the complexes, Co(II) and Cu(II) complexes exhibit max percentage of degradation 85.28 and 84.23, respectively, of MB at 90 min., irradiation of sunlight. The *in vitro* antimicrobial studies revealed that all complexes exhibit significant activities as compared to the ligand. Among the complexes, the highest activity was shown by [Zn-(indal-2-abu)$_2$] against *E. coli,* and *B. subtilis* with an MIC value of 16 μg mL^{-1}. Docking studies against various target proteins revealed that indal-2-abu and its complexes are better candidates for the future development of drugs against many life-threatening bacterial infections.

Supplementary Data

Supplementary data associated with this article are available in the electronic form at http://nopr.niscair.res.in/jinfo/ijca/IJCA_61(03)YYYYYYYY_SupplData.pdf.

Acknowledgment

The authors are gratefully acknowledged to CLIF, University of Kerala, Thiruvananthapuram, SAIF, Cochin, Kerala, CEPCI, Kollam, Kerala, India, for providing the necessary instrumental facilities.

References

1 Abu-Dief A M & Mohamed I M A, *Beni-Suef Univ J Basic Appl Sci,* 4 (2015) 119.
2 Das M, Mukherjee S, Koley B, Choudhuri I, Bhattacharyya N, Roy P, Samanta B C, Barai M & Maity T, *New J Chem*, 44 (2020) 18347.
3 Matsumoto Y, Sawamura J, Murata Y, Nishikata T, Yazaki R & Ryo T, *J Am Chem Soc,* 142 (2020) 8498.
4 Lu L, Wang J, Shi C, Jiang X, Sun Y, Wu W & Hu W, *J Mol Struct,* 1225 (2021) Article 129181.
5 Ali I O, Nassar H S, El-Nasser K S, Bougarech A, Abid M & Elhenawy A A, *Inorg Chem Commun*, 124 (2021) Article 108360.
6 El-Sayed Y S, Gaber M & El-Wakiel N, *J Mol Struct,* 1224 (2021) Article 129283.
7 Nair M S, Arish D & Joseyphus R S, *J Saudi Chem Soc*, 16 (2012) 83.
8 Arish D & Nair M S, *J Coord Chem*, 63 (2010) 1619.
9 Djebbar-Sid S, Benali-BaitichO & Deloume J P, *Polyhedron*, 16 (1997) 175.
10 Kandile N G, Mohamed M I & Ismaeel H M, *J Enzyme Inhib Med Chem,* 32 (2017) 119.
11 Das P & Linert W, *Coord Chem Rev*, 311 (2016) 1.
12 Zhang J, Xu L & Wong W-Y, *Coord Chem Rev*, 355 (2018) 180.
13 Babahan İ, Firinci R, Özdemir N & Gunay M E, *Inorg Chim Acta*, 522 (2021) Article 120360.
14 Zhang Y, Hu Z-Y, Li X-C & Guo X-X**,** *Synthesis*, 51 (2019) 1803.
15 Dong Y, Xue F & Wei Y, *J Phys Chem Solids*, 153 (2021) Article 110007.
16 Mostafa S, Adel MK El-Dean, Mostafa A & Reda H, *Synth Commun*, 48 (2018) 1.
17 Bellamy L J, *The infrared spectra of complex molecules*, Vol 1, 3rd Edition, (Methuen, London) 1980.
18 Deacon G B & Phillips R, *Coord Chem Rev*, 33 (1980) 227.
19 Chauhan H P S, Bhargava A & Rao R J, *Indian J Chem,* 32A (1993) 157.
20 Joseph J, Suman A & Balakrishnan N, *Appl Orgmet Chem*, 31 (2017) e3585.
21 Morris G M, Goodsell D S, Halliday R S, Huey R, Hart W E, Belew R & Olson A J, *J Comput Chem,* 19 (1998) 1639.
22 Trott O & Olson A J, *J Comput Chem,* 31 (2010) 455.
23 Takahara S, Nakagawa K, Uchiyama T, Yoshida T, Matsumoto K, Kawasumi Y, Mizuguchi M, Obita T, Watanabe Y, Hayakawa D, Gouda H, Mori H & Toyooka N, *Bioorg Med Chem Lett*, 28 (2018) 441.
24 Burkhard P, Dominici P, Borri-Voltattorni C, Jansonius J N & Malashkevich V N, *Nat Struct Biol,* 8 (2001) 963.
25 Prashanthi Y, Kiranmai K, Subhashini N J P & Shivaraj *Spectrochim Acta A***,** 70 (2008) 30.
26 Radecka-Paryzek W, Pospieszna-Markiewicz I & Kubicki M, *Inorg Chim Acta*, 360 (2007) 488.
27 Sherer B A, Hull K, Green O, Basarab G, Hauck S, Hill P, Loch JT, Mullen G, Bist S, Bryant J, Boriack-Sjodin A, Read J, Degrace N, Uria-Nickelsen M, Illingworth R N & Eakin A E, *Bioorg Med Chem Lett*, 21 (2011) 7416.
28 Lagunin A, Stepanchikova A, Filimonov D & Poroikov, *J Bioinform*, 16 (2000) 747.
29 Geary W J, *Coord Chem Rev*, 7 (1971) 81.
30 Nakamoto K, *Infrared spectra of inorganic and coordination compounds,* 5th Edition, (Wiley Interscience, New York) 1997.
31 Sharma P K &, Dubey S N, *Indian J Chem*, 33A (1994) 1113.
32 Sakiyan I, Gunduz N & Gunduz T, *Synth React Inorg Met Org Chem,* 31 (2001) 1175.
33 Panchal P K & Patel M N, *Synth React Inorg Met Org Chem,* 34 (2004) 1277.
34 Joseyphus R S & Nair M S, *Mycobiology*, 36 (2008) 93.
35 Venanzi L M, *J Inorg Nucl Chem,* 8 (1958) 137.
36 Joseyphus R S, Dhanaraj C J & Nair M S, *Transition Met Chem*, 31 (2006) 699.
37 Guo Y, Hu X, Zhang X, Pu X & Wang Y, *RSC Adv*, 9 (2019) 41737.
38 Garribba E & Micera G, *J Chem Edu,* 83 (2006) Article 1229.
39 Aziz A & Lal A R, *Arabian J Chem,* 10 (2017) S901.
40 Kivelson D & Neiman R, *J Chem Phys*, 35 (1961) 149.
41 Babu V S, Ramesh A, Raghuram P & Naidu R R, *Polyhedron*, 1 (1982) 607.
42 Arun S & Dutta R L, *Elements of Magnetochemistry, 2nd Edition,* (Affiliated East-West Press, New Delhi) 1993.
43 Nishat N & Malik A, *Arabian J Chem,*9 (2016) S1824.
44 Rauf M A & Ashraf S S, *Chem Eng J*, 151 (2009) 10.
45 Shafaatian B, Ozbakzaei Z, Notash B & Rezvani S A, *Spectrochim Acta A,* 5 (2014) 248.
46 Morris G M, Huey R, Lindstrom W, Sanner M F, Belew R K, Goodsell D S & Olson A J, *J Comput Chem*, 30 (2009) 2785.
47 Singh K, Kumar Y & Pundir R K, *Synth React Inorg Met Org Chem,* 40 (2010) 836.
48 Sinha B, Bhattacharya M & Saha S, *J Chem Sci*, 131 (2019) 19.